Nuclear Instruments and Methods in Physics Research A 390 (1997) 251–256

ELSEVIER

NUCLEAR INSTRUMENTS & METHODS IN PHYSICS RESEARCH Section A

Geometrical parameters of a detection system: A Monte Carlo approach

V.P. Likhachev[1], M.N. Martins*, J.D.T. Arruda-Neto, C.C. Bueno[2], M. Damy de S. Santos[2], I.G. Evseev[4], J.A.C. Gonçalves[2], O.A.M. Helene, S.A. Paschuk[3], H.R. Schelin[3]

Laboratório do Acelerador Linear, Instituto de Física da Universidade de São Paulo, Caixa Postal 66318, 05315-970, São Paulo, SP, Brazil

Received 19 June 1996

Abstract

This work presents a method for the evaluation of dynamic coincidence solid angles for 2π-detector arrangements with large illuminated target area or volume, based on Monte Carlo simulation. Particular constructions useful for photonuclear experiments, using film and gas targets, are considered.

1. Introduction

New theoretical approaches [1,2] for the description of polarization observables of two-particle photodisintegration of light nuclei motivate the interest to make measurements at low photon energies, where experimental results are practically absent [3]. Such kind of experiments require quasimonochromatic photon beams and can be carried out on high duty-factor electron accelerators, associated with the photon tagging technique [4,5]. However, the tagged photon flux is limited to a maximum of about $10^7\,s^{-1}$. Low photon flux and small cross sections require a 2π-detection system and large illuminated target area or volume in order to maximize the photoreaction yield. Other requirements of this kind of experiment are

(i) measurement of energy spectra of both disintegration fragments;

(ii) use of very thin film or low-density gas targets in order to allow the coincidence detection of two particles emitted in opposite directions.

The procedure for the extraction of the differential cross section, $d\sigma/d\Omega$, from the measured yields of two-particle photodisintegration, involves, in the case of extended targets, a sophisticated evaluation of the average solid angles [6,7], even for single-arm measurements. Some particular cases for such calculations were considered in Refs. [8–10].

Two-arm measurements make the problem yet more complicated because it is necessary to take into account the reaction kinematics, that may drastically change the efficiency of the detection system. Moreover, the theoretical analysis of the data is usually done in the center of mass system (CM). The attempt to calculate analytically the average dynamic coincidence solid angles leads to ambiguities in the solutions and huge difficulties, which arise from multiple integrations over the spatial boundaries of the target and detectors [11]. A more reasonable way is to obtain the required data by Monte Carlo simulation [12] of the two-particle photodisintegration events. For this purpose we developed a computer code, which involves not only the experimental setup geometry, but also the physical parameters of the reaction that allows to obtain the average dynamic coincidence solid angles in the CM system, even for complicated detector arrangements.

* Corresponding author. E-mail: martins@if.usp.br.

[1] On leave from Kharkov Institute of Physics and Technology, Kharkov, Ukraine. Supported by CNPq under grant number 300961/93-6.

[2] Instituto de Pesquisas Energéticas e Nucleares, CNEN-SP, São Paulo, SP, Brazil.

[3] Centro Federal de Educação Tecnológica do Paraná, Curitiba, PR, Brazil.

[4] Kharkov Institute of Physics and Technology, Kharkov, Ukraine.

PII S0168-9002(97)00353-7

2. Definitions

The number of coincidences for the two-particle photodisintegration can be written in the following form:

$$N = \int \left\langle \frac{d\sigma^{cm}}{d\Omega}(\theta, \varphi, E_\gamma) \right\rangle N_\gamma(x, y) N_n \Delta\Omega^{i,j}_{cm}(x, y, z)\, dx\, dy\, dz, \tag{1}$$

where $\langle (d\sigma^{cm}/d\Omega)(\theta, \varphi, E_\gamma)\rangle$ is the differential cross section in the center of mass system, averaged over the detectors acceptances, $\Delta\Omega^{i,j}_{cm}(x, y, z)$ is the dynamic solid angle subtended by the detector pair (i, j), from the point with coordinates (x, y, z), considering the reaction kinematics, $N_\gamma(x, y)$ is the photon flux density, and N_n is the target density.

On the other hand,

$$N = \left\langle\left\langle \frac{d\sigma^{cm}}{d\Omega} \right\rangle\right\rangle N^\circ_\gamma N^\circ_n \langle \Delta\Omega^{i,j}_{cm}\rangle, \tag{2}$$

where $\langle\langle (d\sigma^{cm}/d\Omega)\rangle\rangle$ is the differential cross section in the center of mass system, averaged over the detectors acceptances and over the target volume, $\langle \Delta\Omega^{i,j}_{cm}\rangle$ is the dynamic solid angle subtended by the detector pair, averaged over the target volume; N°_γ is the photon flux; and N°_n is the number of nuclei per cm^2 of the target. It is important to notice that

$$\left\langle\left\langle \frac{d\sigma^{cm}}{d\Omega} \right\rangle\right\rangle \equiv \frac{1}{V}\int_V \left\langle \frac{d\sigma^{cm}}{d\Omega} \right\rangle \frac{\Delta\Omega^{i,j}_{cm}(x, y, z)}{\langle \Delta\Omega^{i,j}_{cm}\rangle}\, dV,$$

so that the average of the cross section over the target volume, V, is weighted on the solid angle subtended by the detector pair for each point of the target volume. In this way, the average is actually done over an effective target volume, where the solid angle is not zero. Since photonuclear cross sections usually present smooth angular dependences, this average is a good representation of the cross section in that small region.

The aim of the Monte Carlo simulation is to obtain $\langle \Delta\Omega^{i,j}_{cm}\rangle$ using the correlation between the emission angles, according to the reaction kinematics. The statistical uncertainties of the Monte Carlo simulation results have to be much less than the required accuracy of the differential cross sections, in order to have a negligible contribution to the overall uncertainties.

3. Description of the computer code

The code was written in FORTRAN-77, version 5.3. The input parameters are: beam spot shape and dimensions and tilt angle of the target (film target case) or length of the target (gas target case). In the first step three coordinates are randomly generated, determining the photon–nucleus interaction position in the lab system; see Fig. 1 (in the case of a film target, only two are needed). Then, in the center of mass system, we generate randomly and uniformly, for each event, the polar ($\cos\theta^{cm}$) and azimuthal (φ^{cm}) angles of one of the reaction products and calculate the angles of the other. So, now we have the angles θ^{cm} and φ^{cm} for both particles. The next step is the transformation of these emission angles from the CM to the lab system, according to the reaction kinematics

$$\theta^{lab}_a = \operatorname{arctg}\left(\frac{1}{\gamma_c}\frac{\sin\theta^{cm}_a}{\chi_a + \cos\theta^{cm}_a}\right),$$
$$\theta^{lab}_b = \operatorname{arctg}\left(\frac{1}{\gamma_c}\frac{\sin\theta^{cm}_a}{\chi_b - \cos\theta^{cm}_a}\right), \tag{3}$$

where

$$\gamma_c = \frac{S + M_A^2}{2M_A\sqrt{S}}, \quad \chi_{a,b} = \frac{\beta_c}{\beta_{a,b}},$$

$$\beta_{a,b} = \frac{P^*}{E^*_{a,b}} \quad \text{and} \quad \beta_c = \frac{S - M_A^2}{S + M_A^2}.$$

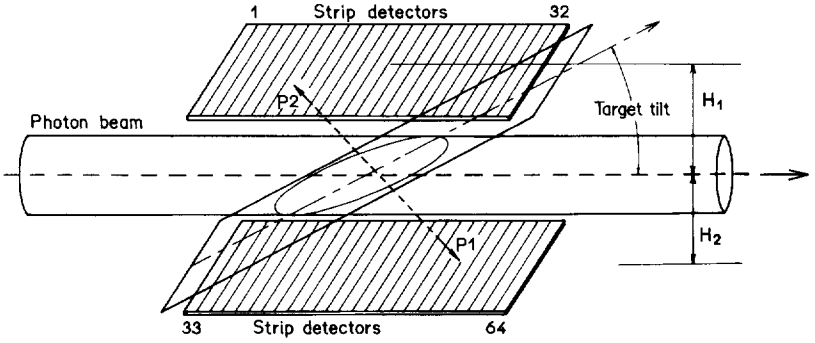

Fig. 1. Schematic view of the strip detector arrangement with a film target.

M_A, M_a and M_b are the masses of the target nucleus and of fragments a and b, respectively, and

$$P^* = \left[\frac{(S - M_a^2 - M_b^2)^2 - 4M_a^2 M_b^2}{4S}\right]^{1/2},$$

$$S = M_A^2 + 2E_\gamma M_A \quad \text{and} \quad E_{a,b}^2 = \sqrt{(P^*)^2 + M_{a,b}^2}.$$

Having the reaction position and the emission angles of each particle in the lab system, the last step is the determination of the coordinates where the particles trajectories hit the planes where the detectors are located, and the analysis of the boundary conditions. As a result, the code delivers four countings: N_i and N_j are the number of particles detected, respectively, by detectors i and j; $N_{i,j}$ the number of coincidences; and N the number of undetected particles.

So, the sorting of the emission angles of the particles is done in the CM system, but the analysis of the boundary conditions (to determine whether the particles hit or not the detectors) is done in the lab system, where it can be done in a simple way. In such an approach, the CM system average coincidence solid angle is

$$\Delta\Omega_{\text{cm}}^{i,j} = \frac{N_{i,j}}{N_{\text{ms}}} 4\pi,$$

where N_{ms} is the number of Monte Carlo starts.

4. Testing the computer code with the film target case

To check the code and to understand the influence of the main geometrical parameters in the coincidence efficiency, we reproduced the result of an analytical calculation [6,7] for the single-arm average solid angle and calculated a simple coincidence case: photofission of ^{238}U.

4.1. Comparison with the analytical calculation

Table 1 presents the results for the single-arm average solid angle subtended by a circular 10 mm diameter detector, located 10 mm away from a circular, uniform and isotropic source, as a function of source diameter. Source and detector are centered over the same axis.

Table 1
Comparison between analytical calculation and Monte Carlo results

Source diameter (mm)	Solid angle (sr)	
	Monte Carlo (this work)	Analytical calculation (Ref. [7])
2.0	0.659 (1)	0.6599
3.0	0.634 (1)	0.6341
6.0	0.558 (1)	0.5589
9.0	0.465 (1)	0.4653
12.0	0.376 (1)	0.3766
15.0	0.302 (1)	0.3030

In the analytical calculation [7], the determination of the single-arm average solid angle of the disc is approximated using the analytical expression for the solid angle of an n-sided regular polygon of the same area. In the Monte Carlo simulation the circular source is used directly. The estimated accuracy of the analytical calculation is 0.1%. Statistical uncertainties of our simulation are about 0.2%. There is an excellent agreement between both results.

4.2. Simulation of the coincidence case

The simulation of the photofission of ^{238}U, monitored by two opposite circular detectors (10 mm diameter) located 30 mm away from each side of the target, is discussed in this section. In this case the CM and lab systems coincide.

Fig. 2(a) presents the count rates for each individual detector and the coincidence count rate versus the distance from a 45°-tilted target to one of the detectors, which is movable. The beam diameter in this case is

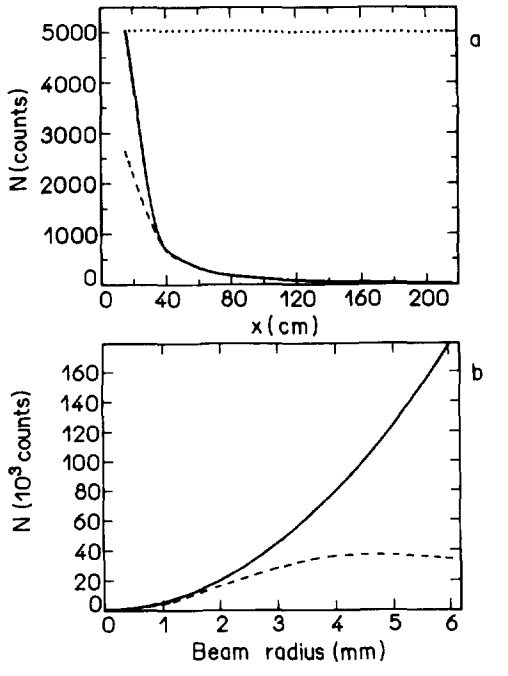

Fig. 2. Results of Monte Carlo simulations for the count rate dependences: (a) versus the target–detector distance (dashed curve: coincidence counts; solid curve: movable detector counts; dotted curve: fixed detector); (b) versus beam radius (dashed curve: coincidence counts; solid curve: singles counts of one of the detectors).

5 mm. The target tilt angle is defined as the angle between the beam direction and the plane of the target (see Fig. 1). For asymmetric positioning, the coincidence count rate is determined by the count rate of the farthest detector and, beyond a certain distance (40 cm in our case, see Fig. 2(a)), both count rates approximately coincide. So, when we take away one of the detectors to infinity, both the singles rate of this detector and the coincidence rate coincide and become zero, but the count rate of the other detector does not change (see dotted curve in Fig. 2(a)). This result is in itself a positive test of the computer code.

Fig. 2(b) shows the singles count rate for each of the detectors and their coincidence count rate as a function of the photon beam radius, for a 45° tilted target. We assume a constant beam intensity per unit area and the singles count rate (solid line in Fig. 2(b)) is roughly proportional to the square of the beam radius. Fig. 2(b) also shows that the coincidence count rate saturates at a beam radius of about 4 mm. Illuminated target areas beyond this radius will contribute only to random coincidences, since only the single count rates increase.

5. Geometry analysis of a strip detector arrangement

The geometry optimization of a detection/target system can be described as an improvement of the geometrical parameters of the detecting array and target in order to minimize the uncertainties of the measured quantities (like cross section, Σ-asymmetry, and others), obtained for a fixed acquisition time, taking into account the physical requirements and characteristics of the experiment (angular resolution, beam, target and detectors dimensions and so on).

It is clear that the space-extended character of the target restricts the angular definition that can be achieved in a single-arm angular distribution experiment. On the other hand, for a reaction with a well-defined kinematics, it is interesting to install a second detection arm and make a coincidence measurement. In this case the cross section is determined from experimental data obtained in double-average view (see item 3), including kinematical effects, allowing a much better angular definition, since it is possible to trace back the reaction position in the target and to define which angles (θ, φ) contribute to the cross section measured by each detector pair.

The aim of this item is to optimize the detector/target geometry and to obtain (i) polar and azimuthal angular distributions on phase plane, and (ii) the average dynamic coincidence solid angle for each detector pair. Monte Carlo simulation is the only practical way to get this information.

The main characteristics of the strip detectors and associated electronics were presented in a previous paper [13]. Here we will be concerned with the relevant geometrical parameters of the arrangement as a whole. We will divide our discussion in two parts, dealing with the film and gas target cases, respectively.

5.1. Film target case

Here we study the expected behavior of an experiment involving a simple angular distribution of photofission fragments, supposing a film target allowing both fragments to be emitted in opposite directions. In this case, the CM and lab systems coincide. The optimized beam–target–detector geometry (for unpolarized photons) corresponds to (see Fig. 1): $H_1 = H_2 = 16$ mm, beam dimensions are 30×30 mm^2 and the target tilt is 17°.

The final results for the angular distribution simulation are shown for some extreme cases of strip positioning: (i) opposite strips (without shift along beam direction), corresponding to $\theta_{lab} = 90°$, Figs. 3(a)–(c) and (ii) oblique strips (maximum shift along beam direction), corresponding to $\theta_{lab} = 22°$ and 158°, Figs. 4(a) and (b). All other cases lie between these ones. Figs. 3 and 4 show that the polar angle subtended by the detector pair spans a range of $\pm 4°$ around its mean value, while the azimuthal angle lay inside a $\pm 45°$ interval.

As mentioned before, the knowledge of the average dynamic coincidence solid angle of each strip pair is necessary for the experimental data analysis. The results obtained from the simulations are presented in Table 2. We can see that the calculated efficiencies of the strip pairs vary about 40 times through the range of strip coordinates. The maximum value is reached for opposite strips facing the middle of the target, while opposing strips that face the limits of the target are about 15% less efficient. It is interesting to note that this difference becomes much larger if the target is illuminated by a narrow (along the target length) beam. Strip pairs close to the middle of the target are much more sensitive to the dimensions of the illuminated target area than the strips close to the extremes of the target, as shown in Fig. 5. The largest solid angle difference occurs between the strip pairs (1–64) and (32, 33), corresponding to the two extreme oblique cases. This difference arises mostly because of the effective target area that corresponds to the whole target in the first case and is very small (a thin transversal strip in the middle region of the target) in the second one. This difference will not occur in an actual experimental situation, because the large solid angle of the first case comes from events in which the particles were emitted almost parallel to the target surface, thus subject to high energy losses.

The singles count rates are about 20 times higher than the coincidence rates for opposite strips and do not vary so much with strip position.

The total dynamic coincidence solid angle can be evaluated as $\Omega_{total} = 4\pi(\sum_{ij} N_{ij})/N_{ms}$, where N_{ij} is the number of coincidence counts between strips i and j and

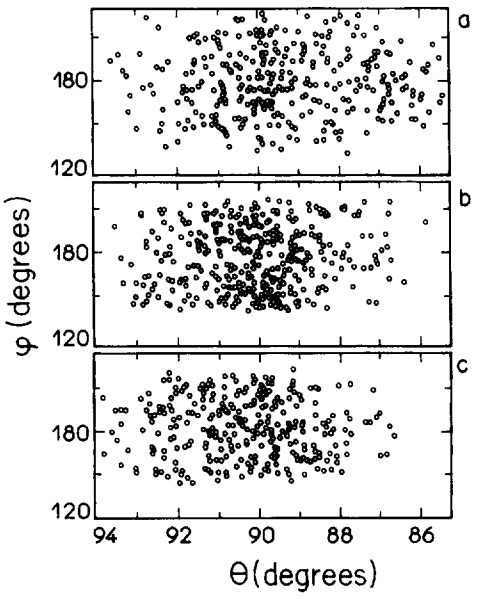

Fig. 3. θ and φ phase plane for film target and (a) strip pair 32–64 ($\theta_{lab} = 90°$, target working area is close to the upper detector plane); (b) strip pair 16–16 ($\theta_{lab} = 90°$, target working area is located midway between the detector planes); (c) strip pair 1–33 ($\theta_{lab} = 90°$, target working area is close to the lower detector plane).

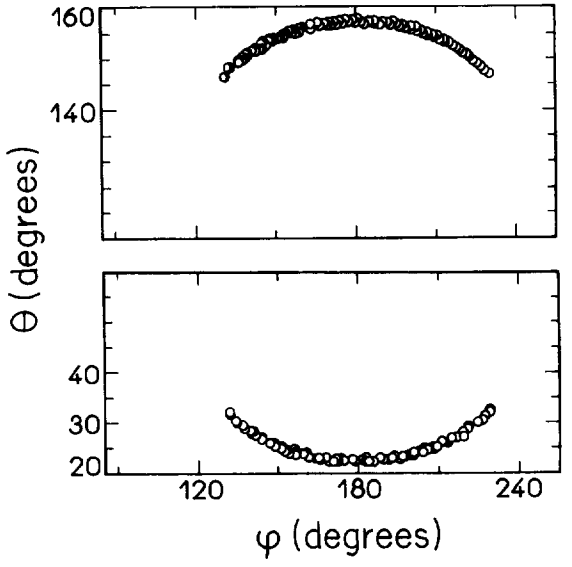

Fig. 4. θ and φ phase plane for film target and (a) strip pair 32–33 ($\theta_{lab} = 22°$, particle emission direction is almost parallel to the target. Effective target area is very close to the whole target surface); (b) strip pair 1–64 ($\theta_{lab} = 158°$, very small effective target area).

Table 2
Angular acceptances and average dynamic coincidence solid angles for some strip pairs of a 2π-detector arrangement, working with a film target and detecting fragments from photofission

Detector pair	θ_{min}–θ_{max} (degree)	φ_{min}–φ_{max} (degree)	$\Delta\Omega$ (10^{-3} sr)
1–33	86.5–93.5	130–225	7.78 (5)
16–48	86.5–93.5	140–215	9.36 (6)
32–64	86.5–93.5	130–225	7.77 (5)
1–64	148–158	130–230	8.139 (5)
32–33	22–32	130–230	0.20 (1)

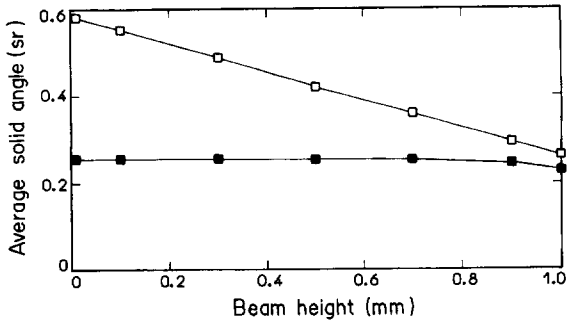

Fig. 5. Average dynamic coincidence solid angles for detector pairs (16–48), squares, and (1–33), dark squares, as a function of beam height. Taking as reference the point where the line joining detectors 1 and 33 crosses the target, the beam spot was centered 1 mm above this point in the first case and 16 mm above in the second one. The target tilt angle is 17°.

N_{ms} is the number of Monte Carlo starts. For the case of photofission, the setup discussed above presents a total dynamic coincidence solid angle of about 20% of 4π.

5.2. Gas target case

In this case we study the behavior of a photodisintegration experiment performed with polarized photons, namely $\vec{\gamma}(^3\text{He}, \text{pd})$. The geometrical parameters are $H_1 = H_2 = 31$ mm, beam size equals 30×60 mm^2 and target length is 100 mm. The detector–target distance was increased in this case to improve the azimuthal angular definition, since the ability to extract the Σ-asymmetry depends on this parameter. The increase in the detector–target distance, on the other hand, decreases the statistics, so the final distance is obtained by a compromise between the two parameters.

In this case there is a significant difference between the expected angular distributions observed in the CM and lab systems, especially in the near-threshold region. Consequently, all the characteristics that are being discussed, like phase plane angular distributions, average dynamic

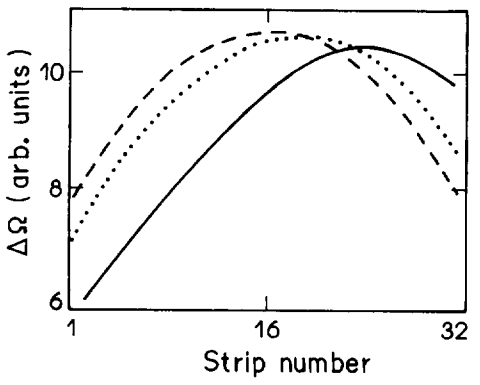

Fig. 6. Average dynamic single-arm solid angle as a function of strip number for the reaction $\vec{\gamma}(^3\mathrm{He}, \mathrm{pd})$ and $E_\gamma = 5.5$ MeV (solid curve), 6 MeV (dotted curve) and 14 MeV (dashed curve).

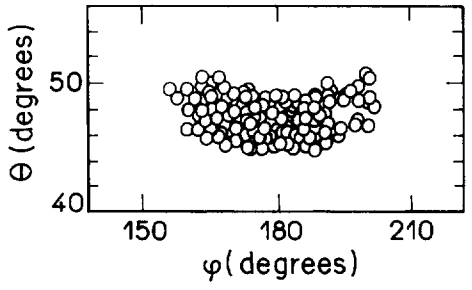

Fig. 7. (θ, φ) phase plane for gas target and strip pair 1–64 ($\theta_{cm} = 47°$).

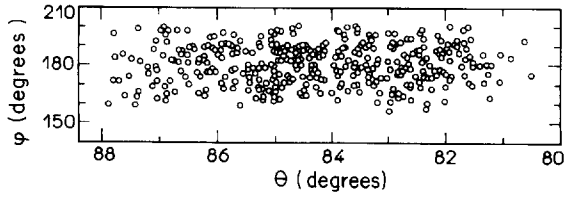

Fig. 8. (θ, φ) phase plane for gas target and strip pair 1–33 ($\theta_{cm} = 84°$).

coincidence solid angle and even dynamic single-arm solid angle depend on the incident photon energy. Fig. 6 shows the dynamic single-arm solid angle, as a function of strip number, for three photon energies. The dependence with strip number is clearly asymmetric for $E_\gamma = 5.5$ MeV (close to the threshold), becoming symmetric at $E_\gamma = 14$ MeV.

Figs. 7 and 8 show the (θ, φ) phase plane for the two extreme combinations of detector pairs, namely pairs (1–33) and (1–64). All other combinations lie between these. The results show that (i) polar angles are within a $\pm 4°$ interval for opposing pairs and within a $\pm 8°$ interval for the extreme oblique case; and (ii) azimuthal angles for all combinations are within a $\pm 20°$ interval. The total dynamic coincidence solid angle corresponds to 14% of 4π, for $E_\gamma = 6$ MeV.

6. Conclusions

We presented a Monte Carlo method for the determination of average dynamic solid angles and also for the study of the relevant geometrical parameters of 2π-detector arrangements for coincidence measurements.

A detailed consideration of the particular constructions for film and gas targets shows that moderate angular resolution can be achieved even with large illuminated target area or volume and large total solid angle. This is a very important characteristic to be considered in the design of two-particle photodisintegration experiments where the particles are measured in coincidence. Accurate determination of the dynamic solid angles is of fundamental importance for the experimental data analysis of such experiments.

References

[1] V.V. Kotliar, A.V. Shebeko, Sov. J. Nucl. Phys. 45 (1987) 984.
[2] A.A. Zayats et al., Sov. J. Nucl. Phys. 57 (1994) 798.
[3] Yu.V. Vladimirov et al., preprint KhFTI 89-19, Moscow, 1989.
[4] L.S. Cardman, Proc. of the Magnetic Spectrometer Workshop, Williamsburg, Virginia, USA, 1983.
[5] J.-O. Adler et al., Nucl. Instr. Meth. A 294 (1990) 15.
[6] R.P. Gardner et al., Nucl. Instr. and Meth. 176 (1980) 615.
[7] R.P. Gardner, K. Verghese, Nucl. Instr. and Meth. 93 (1971) 163.
[8] K. Verghese et al., Nucl. Instr. and Meth. 101 (1972) 391.
[9] M. Belluscio et al., Nucl. Instr. and Meth. 114 (1974) 145.
[10] M.V. Green et al., Nucl. Instr. and Meth. 117 (1974) 409.
[11] R.A. Rizk et al., Nucl. Instr. and Meth. 245 (1986) 162.
[12] L. Wielopolski, Nucl. Instr. and Meth. 226 (1984) 436.
[13] V.P. Likhachev et al., Nucl. Instr. and Meth. A 376 (1996) 455.